Available online at www.sciencedirect.com
ScienceDirect
Journal of the European Ceramic Society 29 (2009) 3279–3287
www.elsevier.com/locate/jeurceramsoc

Investigation of the morphological changes promoted by heating of Si–C–O ceramics derived from a phenyl-rich hybrid polymer. Effect of Ni in the polymeric precursor

Mariana Gava Segatelli [a], Eduardo Radovanovic [b], Maria do Carmo Gonçalves [a], Inez Valéria Pagotto Yoshida [a,*]

[a] *Institute of Chemistry, University of Campinas - UNICAMP, 13083-970 Campinas, SP, Brazil*
[b] *Department of Chemistry, University of Maringá - UEM, 6165, 87020-900 Maringá, PR, Brazil*

Received 24 April 2009; received in revised form 26 May 2009; accepted 11 June 2009
Available online 8 July 2009

Abstract

This study focuses on the structural and morphological changes promoted by heating of silicon oxycarbide ceramics obtained from hybrid polymeric precursors based on poly(methylsiloxane) and divinylbenzene, with or without nickel acetate, by pyrolysis under Ar at different temperatures. The increase of the temperature from 950 to 1500 °C promoted the densification and crystallization of SiC and graphite nanodomains in the ceramic bulk with or without Ni, as identified by HRTEM. Moreover, the Ni-containing precursor led to the formation of ultra-long amorphous nanowires on the surface and voids in the ceramic body obtained at 1500 °C. These nanowires presented different sizes and morphologies, but similar compositions, basically composed by silicon and oxygen, with the presence of carbon at their external layers. The growth mechanism and the nature of the nanowires are also proposed. The addition of nickel acetate in the polymeric precursor induced the formation of nanowires with different morphologies in the Si–O–C system.

Keywords: Electron microscopy; SiC; SiO_2; Glass ceramics; Nanowires

1. Introduction

The pyrolysis of polymers has widely been used in the preparation of ceramic materials, due to its versatility in relation to the classical powder processing routes that are usually employed in the manufacturing of oxide and non-oxide ceramics.[1] In the classical routes, the solid-state reactions occur at high temperatures and the final products usually contain microparticles of polydisperse sizes, poor chemical homogeneity and undesirable phases, as a consequence of the low diffusion coefficients of the starting reagents.[2] On the other hand, the possibility to tailor materials with better structural homogeneity at relatively lower temperatures and associated to the traditional polymer processing techniques, makes polymer-derived ceramics an attractive route. In addition, this route is suitable to produce ceramic materials in different shapes, such as fibers, films, monolithic bodies and coatings.[3]

Among the several polymeric precursors available, the polysiloxanes are considered the most attractive to obtain silicon oxycarbide ceramics, described as SiC_xO_{4-x}, where $0 \leq x \leq 4$, or simply SiC_xO_y or SiCO, by the pyrolysis process.[4,5] At 1000 °C, such ceramics are characterized as a metastable material constituted by a random distribution of different silicon sites, such as SiO_4, SiO_3C, SiO_2C_2, $SiOC_3$ and SiC_4, known as Q, T, D, M and C units, respectively. In addition, a dispersed free carbon phase, C_{free}, is often found as a secondary carbon phase.[6] The chemical structure of these materials only contains Si–O and Si–C bonds, while Si–Si and C–O bonds are not usually present.[7,8] Subsequent thermal treatment at temperatures exceeding 1000 °C initiates the evolution of SiO and CO gases that, associated with the redistribution reactions between the different silicon sites, promotes the local crystallization of thermodynamically stable phases in the non-crystalline matrix, such as β-SiC, cristobalite silica (c–SiO_2) and also a C-graphitic

* Corresponding author. Tel.: +55 19 3521 3130; fax: +55 19 3521 3023.
E-mail address: valeria@iqm.unicamp.br (I.V.P. Yoshida).

0955-2219/$ – see front matter © 2009 Elsevier Ltd. All rights reserved.
doi:10.1016/j.jeurceramsoc.2009.06.018

phase. This effect is more pronounced at temperature around or higher than 1300 °C. The first crystallization event is the nucleation of C_{free}, known as basic structural units (BSUs), which is followed by the nucleation of nanosized SiC crystallites embedded in the SiCO matrix.[9] At higher temperatures, the contribution of the carbothermal reduction reaction between SiO_4 and C sites must also be considered.[8,10,11]

The composition of the polymeric precursor, mainly the abundance of organic groups, can also influence the composition of the ceramic product, particularly the amount of C-phase. In addition, it is well established that the incorporation of some transition metals in the precursors can induce the formation of organized structures,[12] also with different morphologies on the micrometric and nanometric scales in non-oxide and C-based materials.[13–17] Leu et al.[13] verified that the addition of nickel was essential for the successful preparation of silicon carbide whiskers from the thermal decomposition of methyltrichlorosilane at 1300 °C. Jou and Hsu[15] synthesized straight and curled carbon nanotubes, CNTs by the pyrolysis of polycarbosilane and iron nanoparticles at temperatures between 800 and 1100 °C. These CNTs showed different morphologies, as functions of the molar mass of the polymeric precursor, as well as typical features of CNTs produced by the conventional gas–solid reactions using carbon vapor or hydrocarbon gases. These nanostructures can also be formed in the pores[12] and on the surface[18,19] of ceramic materials, as well as on the surface of substrates such as mesoporous activated carbon,[20] silicon[21] and SiC and alumina fibers.[22] Among the selected metals for inducing these types of nanostructures, nickel has received special attention due to its catalytic activity in promoting the nucleation of nanotubes and the formation of turbostratic carbon islands dispersed in polymer-derived ceramics,[12] GaN nanowires[23] and nanowires having a SiC core and a SiO_2 shell.[24] The effect of Ni, introduced as nickel acetate in hybrid polymeric precursor derived from poly(methylsiloxane) and divinylbenzene, was recently investigated on the final characteristics of the resulting silicon oxycarbide ceramics.[25] The presence of Ni in the precursor promoted structural changes during the pyrolysis process, mainly in relation to the nucleation of crystalline phases in the ceramic matrix, such as β-SiC, cristobalite silica, graphitic carbon, metallic nickel, NiO and Ni_2Si, when compared with the corresponding ceramic without Ni.

The present study focuses on the structural and mainly the morphological changes promoted by heating of silicon oxycarbide ceramics obtained from hybrid polymeric precursors based on poly(methylsiloxane) and divinylbenzene, with or without nickel acetate, by pyrolysis under an Ar atmosphere at 950, 1300 and 1500 °C. The characterization of crystalline nanodomains dispersed in the ceramic bulk, as well as the chemical composition of the produced nanowires are also reported.

2. Experimental

2.1. Sample preparation

Hybrid preceramic polymers, with and without NiAc, were synthesized by the Pt-catalyzed hydrosilylation reaction between poly(methylsiloxane), PMS, and divinylbenzene, DVB, according to the previously described procedure.[25] The PMS/DVB hybrid polymers were prepared in 1:1 molar ratio, in relation to the –CH=CH_2: Si–H groups, giving rise to polymeric networks containing 1,4-diethylphenylene bridges between siloxane chains. Green polymeric bodies of 13.5 × 1.3 × 0.3 cm, with and without NiAc, were pyrolyzed at 950 °C, under a flowing Ar–atmosphere (100 mL/min), with a heating and cooling rate of 5 °C/min and a holding time of 1 h. The pyrolysis was carried out in an EDG 5P tubular furnace, equipped with an internal alumina tube and a temperature controller. Afterwards, these samples were heated at 1300 and 1500 °C using a Thermolyne F59340-CM tubular furnace, under flowing argon. In this case, the pyrolysis process was conducted on samples previously pyrolyzed at 950 °C. The surface of Ni-containing ceramic samples obtained at 1500 °C presented a felt-like layer of entangled nanowires.

2.2. Morphological evaluation

Both fracture surface and surface morphologies of ceramic samples were examined by field emission scanning electron microscopy (FESEM), using a JEOL JSM-6340F microscope, with a 5 keV accelerating voltage. Prior to analyses, the exposed surface was coated with a thin layer of carbon followed by a gold/palladium alloy, in a Bal-Tec MED 020 equipment, in order to minimize charging under the incident electron beam.

Structural and elemental information of the bulk ceramic samples, with and without Ni, and of nanowires was obtained by high-resolution transmission electron microscopy (HRTEM), using a JEOL JEM 3010 URP microscope, with a 0.17 nm point resolution and a 300 keV operating voltage. The sample preparation for HRTEM consisted of the dispersion of the powdered ceramic samples or of the nanowires in isopropyl alcohol, using an ultrasound process in order to obtain very thin samples from the ceramic matrix or an effective separation of the entangled nanowires. Then, one drop of the solution was put on the copper grid containing a lacey carbon film. After the evaporation of the solvent, the copper grid containing the sample was submitted to analysis. Gatan digital micrograph software, version 3.11.1, was employed for image processing.

The morphologies and elemental distributions of Si, O, C and Ni in the nanowires were also investigated by transmission electron microscopy (TEM) using a Carl Zeiss CEM 902 microscope, with 80 keV accelerating voltage, which was equipped with a Castaing–Henry energy filter spectrometer within the column. Elemental images by electron spectroscopy imaging (ESI) and spectral data by electron energy loss spectroscopy (EELS) were acquired for the elements found in the sample using the three-window method for silicon L-edge, oxygen K-edge and carbon K-edge. The energy-selecting slit was set at 132 eV for Si, 542 eV for O and 303 eV for C with 15 eV slit widths.[26] The sample preparation for ESI consisted of the same procedure used for HRTEM. The images were obtained using a slow scan CD camera (Proscan) and processed in the iTEM universal imaging platform. The energy resolution during EELS spectra acquisition was 2.0 eV.

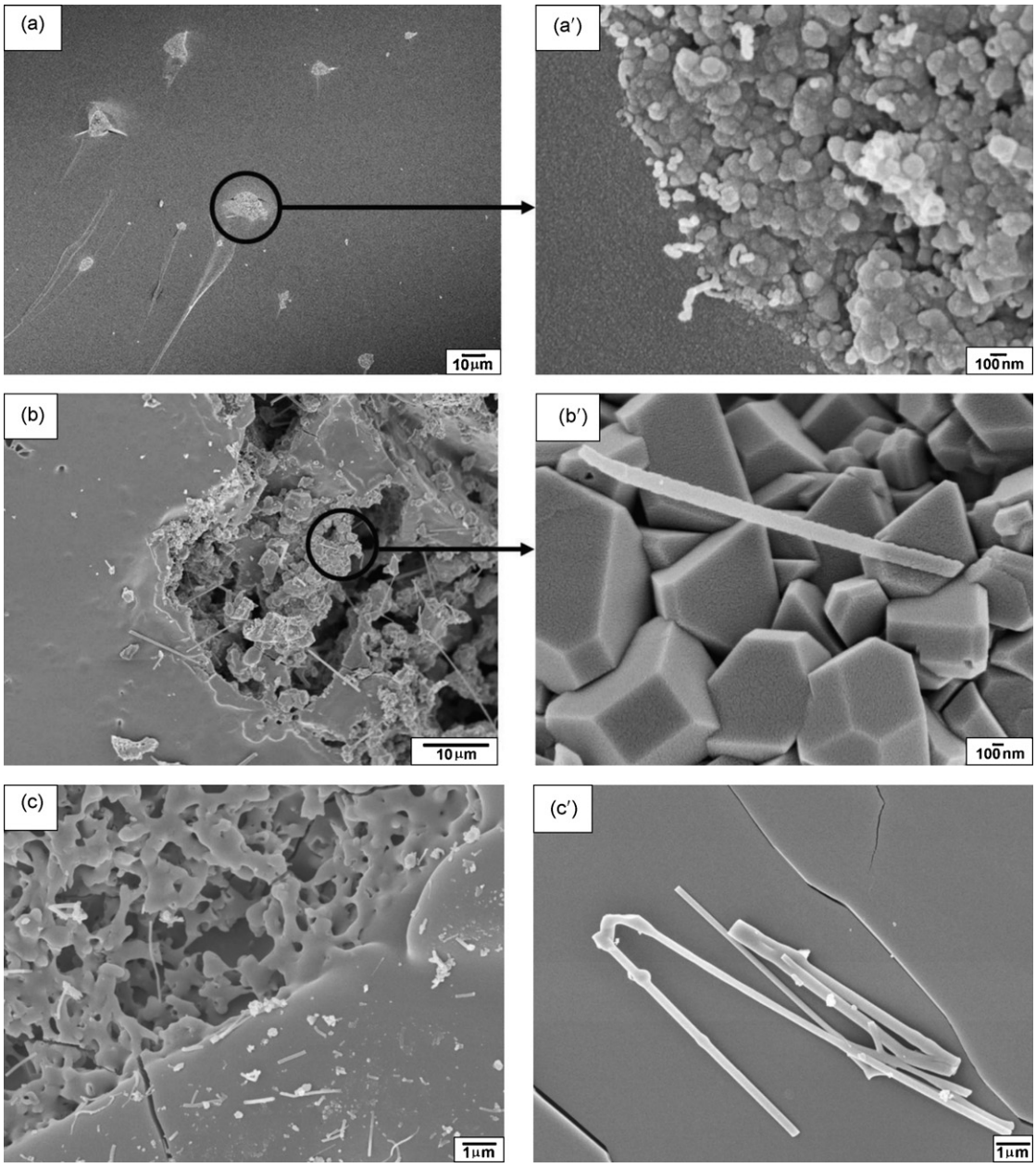

Fig. 1. SEM images of the fracture surface of the Ni-containing ceramic specimens, obtained at 950 °C (a), 1300 °C (b) and 1500 °C (c). a′ and b′ show specific magnified regions and c′ shows a detail of the surface.

3. Results and discussion

3.1. Morphological characterization of the SiCO-based ceramic bulk

The morphology of the SiCO-based ceramic bulk (not shown) presented no significant changes with the different pyrolysis temperatures. It was characterized as being typical of globular and dense materials. However, Ni-containing ceramics, obtained from the same PMS/DVB precursor with NiAc, showed non-uniform morphology with different features at their fracture surface, at all the pyrolysis temperatures, as can be seen in Fig. 1.

The image of the ceramic obtained at 950 °C was characterized by a smooth and dense matrix containing dispersed Ni-rich islands. These islands were made up by Ni-rich globular aggregates (see the magnified area in Fig. 1a′), associated with bright structures, which were assigned to the presence of Ni. In addition, the initial formation of wire-like nanostructures from these aggregates was also observed, which suggests that the Ni acted as a nucleation agent for the formation of these nanostructures. The sample obtained at 1300 °C showed a similar morphology (Fig. 1b) with respect to the matrix profile, except for the presence of a few pores, not observed in the material discussed just above. In these pores, a few straight nanowires, together with microcrystals containing regular hexagonal facets, were also observed (see the magnified area in Fig. 1b′). Li et al.[27] reported the synthesis of SiC nanowires with hexagonal shapes along their growth direction by a sol–gel method with direct heating. In their

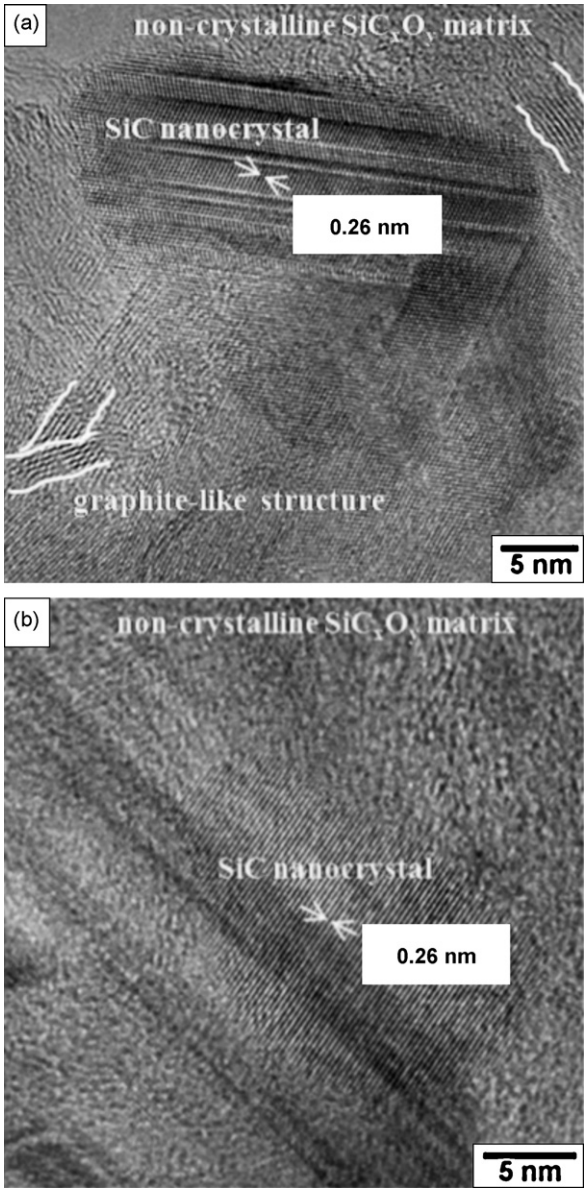

Fig. 2. HRTEM images from the bulk of the ceramic specimens obtained at 1500 °C without Ni (a) and with Ni (b).

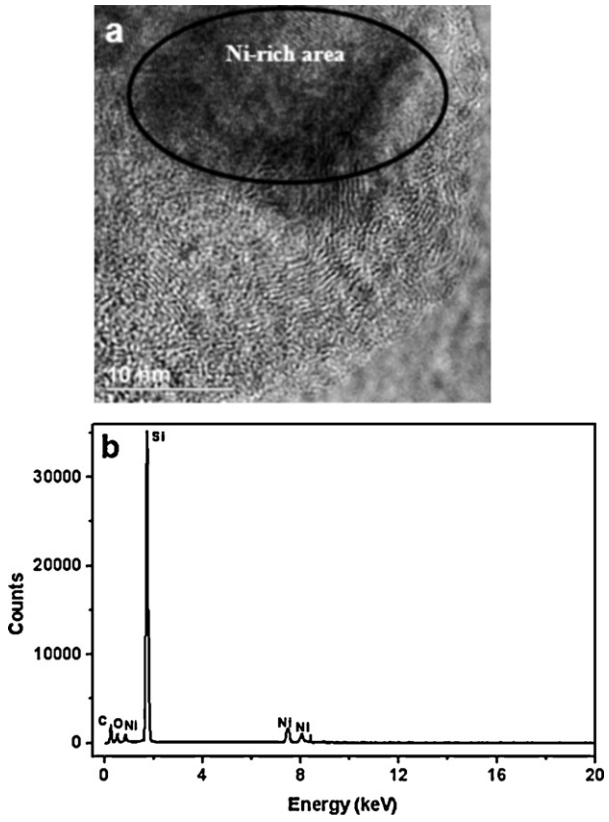

Fig. 3. HRTEM image from the bulk of the Ni-containing ceramic obtained at 1500 °C showing the presence of Ni (a) and EDS spectrum corresponding to the total area (b).

study, morphological evaluation indicated that this new type of SiC nanowire grew from hexagonal facets of SiC nanoparticles during the vapor–solid (VS) growth process. In our ceramic samples pyrolyzed at 1300 °C, the nanowires did not grow from the hexagonal microcrystals, since no micrograph showed this phenomenon. According to the observed morphological profile and XRD patterns (not shown),[25] these microcrystals were probably associated to the SiC phase.[27] On the other hand, the sample pyrolyzed at 1500 °C displayed two distinct regions (Fig. 1c). The first one presents a large number of nanowires dispersed at the fracture surface of the ceramic matrix, while the second reveals a partial softening of the matrix at this temperature range. At this temperature, redistribution reactions between the Si–O and Si–C bonds are favorable, resulting in continuous transformations of the SiC_xO_y phase, due to softening.

HRTEM images of the SiCO ceramic bulk, with and without Ni, pyrolyzed at 1500 °C can be seen in Fig. 2. For both samples, well-formed nanocrystals could be observed. In the absence of Ni, crystalline planes with d-spacing of 0.26 nm corresponding to (1 1 1) planes of β-SiC and C-graphitic domains, with spacing of 0.35 nm assigned to their (0 0 2) planes, embedded in a non-crystalline SiCO matrix, were observed (Fig. 2a). The orientation of the graphite basal planes is indicated by white guidelines. At this temperature range, the formation of SiC is expected as a consequence of the redistribution reactions as well as the carboreduction reactions, as mentioned above. The Ni-containing ceramic (Fig. 2b) also revealed the presence of SiC nanocrystals within the non-crystalline matrix. Although these images showed a bigger SiC nanocrystal in the ceramic sample obtained without Ni, this was not the rule. The main difference between the two samples is that in the Ni-containing ceramic a high amount of crystalline nanodomains, which are generally larger than those in the ceramic without Ni, was observed, as previously determined by the Scherrer equation.[25] Results obtained from the structural study of these ceramics[25] revealed that the Ni acted as a nucleation agent, reducing the activation energy for the crystallization of phases, in comparison to the material without Ni. In the illustrated area of Fig. 2b, the Ni-containing ceramic did not show any evidence of graphitic-C in the material, although this phase had clearly been identified by XRD patterns and ^{13}C NMR analyses.[25] In this way, it can be assumed that the more effective crystallization of SiC in relation to C-graphitic in

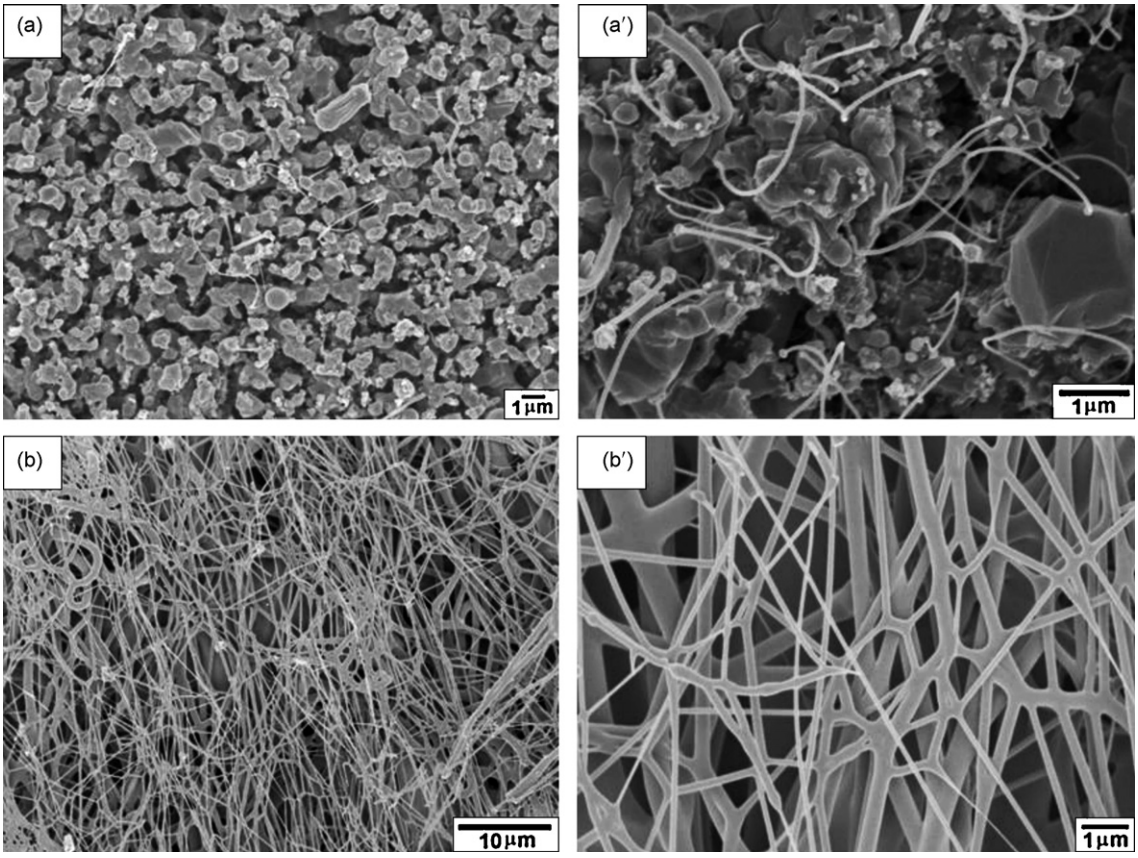

Fig. 4. SEM images at the surface of the ceramic specimens obtained at 1500 °C without Ni (a) and with Ni (b). a′ and b′ are the respective images acquired with higher magnification.

the Ni-containing sample may justify why it was difficult to find this last phase dispersed in the matrix. In order to have a clear distinction of this phase by HRTEM, the graphite lattice planes have to be oriented perpendicularly to the image plane (parallel to the incident electron beam) and the number of layers making up the turbostratic structure has to be large enough (higher than four).[28]

The presence of Ni was identified in the darker regions of the HRTEM image and in the EDS spectrum (Fig. 3a and b). The image shows a Ni-rich region dispersed in the ceramic matrix, with some parallel fringes surrounding it, which can be attributed, probably, to the SiC crystalline phase (upper left side). This observation is in agreement with the Ni nucleation effect, mainly in relation to the formation of the SiC crystalline phase. Scheffler et al.,[12] however, verified that the presence of Ni in poly(methylphenylsilsesquioxane)-derived ceramics promoted an arrangement of the atomic planes of turbostratic carbon around a Ni cluster in the matrix as well as carbon nanotubes in pores after pyrolysis at 1000 °C. According to these authors, the dispersed graphite-like structures were responsible for the higher electrical conductivity in relation to the Ni-free sample.

3.2. Morphological characterization of the SiCO-based ceramic surface

In addition to the effects of different pyrolysis temperatures observed at the fracture surfaces, particularly in the sample obtained at 1500 °C, the presence of NiAc in the hybrid PMS/DVB polymeric precursor resulted in more complex morphologies with distinct features on the surfaces of the final ceramics, as can be seen in Fig. 4.

Fig. 4a shows the morphology at the surface of a ceramic specimen without Ni, showing structures with different features and shapes together with the presence of a few nanowires inserted in these structures, Fig. 4a′. On the other hand, a white felt layer was produced on the surface of the Ni-containing ceramic specimen, as can be seen in Fig. 4b. A large number of nanowires, usually over several micrometers in length with nanometric diameters, indicating a large aspect ratio, were formed. These nanowires were normally straight along their axes but also showed branched structures and/or connectivities between them, as can be seen in Fig. 4b′. Structures connected to each other, resulting in a nanonetwork, were also found in SiC nanowires synthesized from a series of reactions between mixtures of milled Si–SiO_2 powders and C_3H_6 at a relatively low temperature.[29] An explanation of this phenomenon is that, during the SiC nanowire growth process along its axial direction, two tips of the nanowires can meet and, in this way, the nanowires easily generate structural defects at their tips. Consequently, a new nanowire can start to grow from this junction, leading to the formation of a nanonetwork.

Images acquired with higher magnification confirmed that the structures formed on the ceramic surfaces were nanowires (Fig. 5), revealing their amorphous structures (Fig. 5d). These

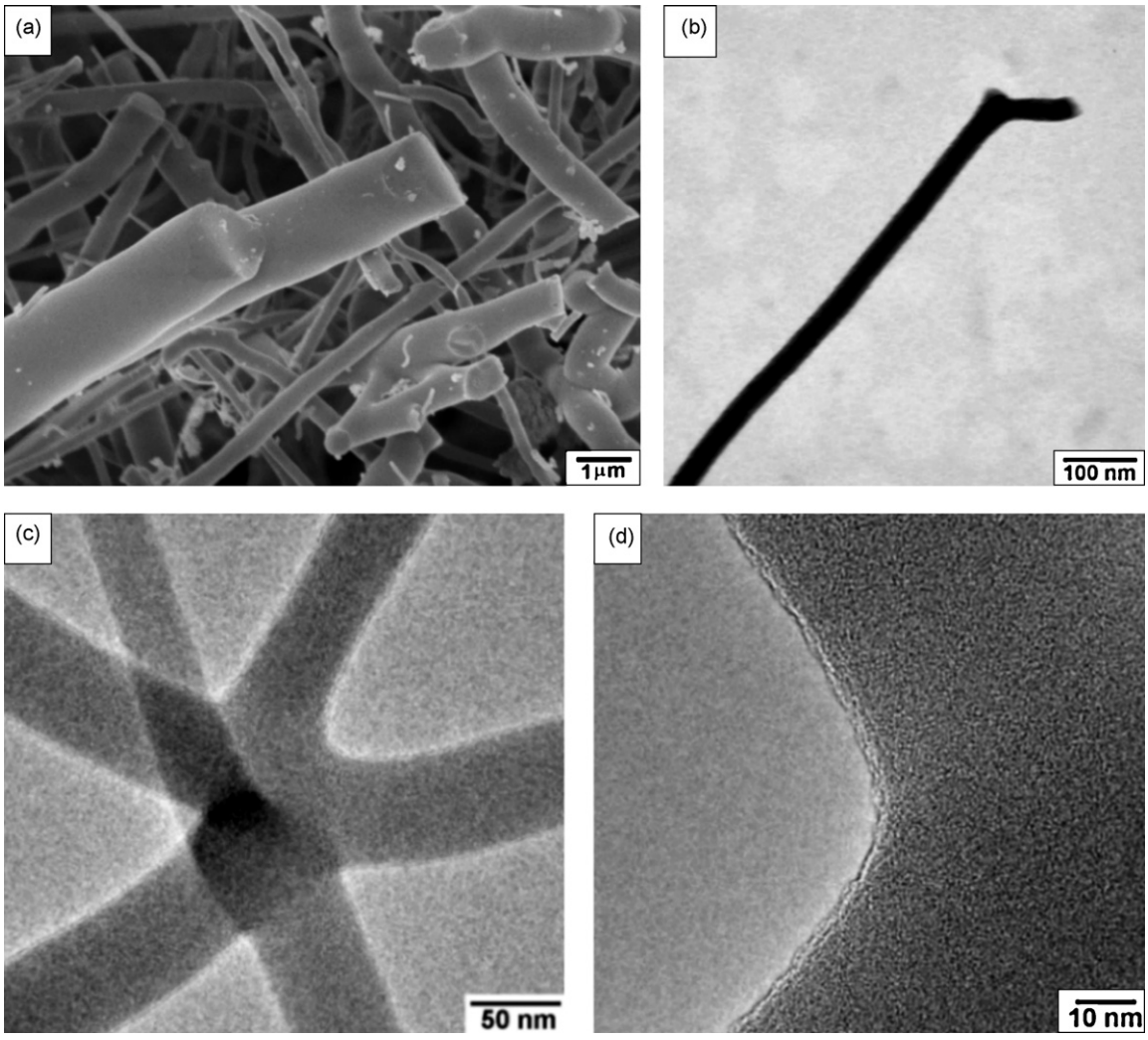

Fig. 5. SEM (a), TEM (b) and HRTEM (c and d) images showing the nanowires formed at the surface of the Ni-containing ceramic specimens. Image (d) illustrates the amorphous structure of the nanowires.

images are also adequate to investigate the growth mechanism of the nanowires produced on the ceramic surfaces, since the tips of the nanowires were clearly observed by SEM and TEM (Fig. 5a and b). As can be observed in these images, there were no bright spherical particles present on the tips of the nanowires, which would be an indication of the presence of nickel. This is a typical feature of nanostructure formation by the vapor–liquid–solid (VLS) growth mechanism.[16,20] In a simple way, a typical VLS process starts with the dissolution of gaseous reactants into nanosized liquid droplets of a metallic catalyst, followed by nucleation and growth of single-crystalline rods and then wires.[30] Thus, according to morphological observations, it can be assumed that the nanowires produced at the ceramic surfaces in this study were not grown by the VLS mechanism. Berger et al.,[24] however, described the in situ growth of SiC/SiO_2 nanowires by the VLS mechanism from poly(organosilsesquioxane) loaded with nickel and silicon. The incorporation of Ni and silicon filler in the precursor was crucial to obtain the nanowires in the resulting ceramic, as the silicon-free material showed the presence of a percolating network of tubostratic graphite and carbon nanotubes. During the pyrolysis process, nickel silicide nanoparticles acted as nuclei for nanowire growth.

Apart from the Ni acting as a crystallization agent, the morphological observations revealed that, in this specific system, it also seems to be a determining component for the induction of the nanowire formation on ceramic specimen surfaces.

3.3. Chemical analysis of the nanowires produced on the ceramic specimen surfaces

The chemical composition of the nanowires with straight and curved shapes was firstly examined by EDS. The spectra showed that both nanowires were basically made up of silicon and oxygen, as can be seen in Fig. 6. Carbon and nickel elements were not observed in their chemical compositions by this technique.

The nanowires were also analyzed by EELS and ESI. Fig. 7a and b illustrate the bright-field TEM images of straight and curved nanowires, respectively, and the corresponding silicon, oxygen and carbon maps. Only these elements were detected in the nanowires, which did not show the presence of Ni. ESI images using the $L_{2,3}$ edge of silicon and K-edge of oxygen

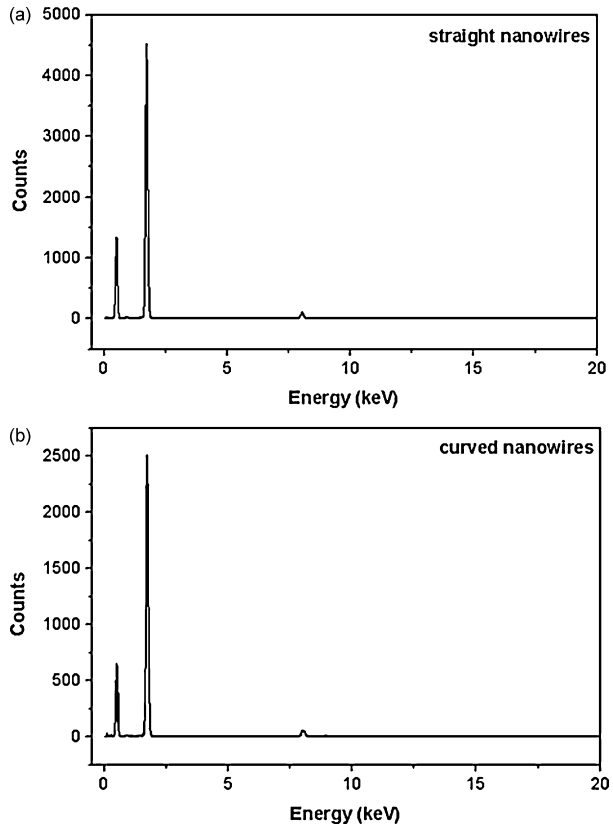

Fig. 6. EDS spectra of the straight (a) and curved (b) nanowires.

showed that silicon and oxygen atoms are uniformly distributed in both nanowire structures. On the other hand, the carbon map obtained from carbon K-edge indicated that this element was more concentrated at the outer nanowire layers. Apparently, there are no significant differences in the chemical composition of both nanowires. The presence of carbon was only verified by EELS and, taking into account that this technique is more sensitive than EDS, mainly for carbon,[31] we considered that the nanowires are also made up of carbon, although in lower amounts.

Fig. 8 shows typical cumulative EELS spectra of the nanowires for the Si, O and C. The spectral profile for each element was similar for both nanowire structures, which can be considered, as presenting no significant changes in their respective compositions. The EELS spectrum of silicon for straight nanowires revealed the presence of its characteristic L-ionization edge, showing a shift of 2 eV toward lower energies in relation to those of curved nanowires. However, this value is within the technique error. The Si–L_{23} silicon edge of for straight nanowires has an edge onset at about 97 eV and two distinct peaks at ~105 eV (α) and 112 eV (β), respectively. In addition, there is a broad peak at about 131 eV (γ), which was also verified for SiO_2 and SiC.[32] In the case of a SiO_2 glass, the Si–L_{23} edge shows an onset at about 104 eV and two separate peaks that are positioned at ~108 and 115 eV, while SiC reveals an onset at about 99 eV and a major peak centered at 102 eV.[32] The first and second peaks found in the silicon spectra are attributed to Si–C and Si–O bonds, respectively, present in the nanowire structure.[33] Lichtenberger and Neumann[34] demonstrated that the first peak in the silicon spectrum, corresponding to SiO_2, is associated to the excitation of a 2p electron into unoccupied $6t_2$ and $6a_1$ states, which exhibit p- and s-like symmetries, respectively. The second peak is related to additional states of higher energies but lower occupancies, which are identified as 2e, $7t_2$ and $7a_1$ with d-, d- and s-like symmetries, respectively. The third observed broad peak originates from molecular excited states inside the molecule.[34]

The oxygen spectrum for straight nanowires revealed a shift of 5 eV toward higher energies when compared to curved

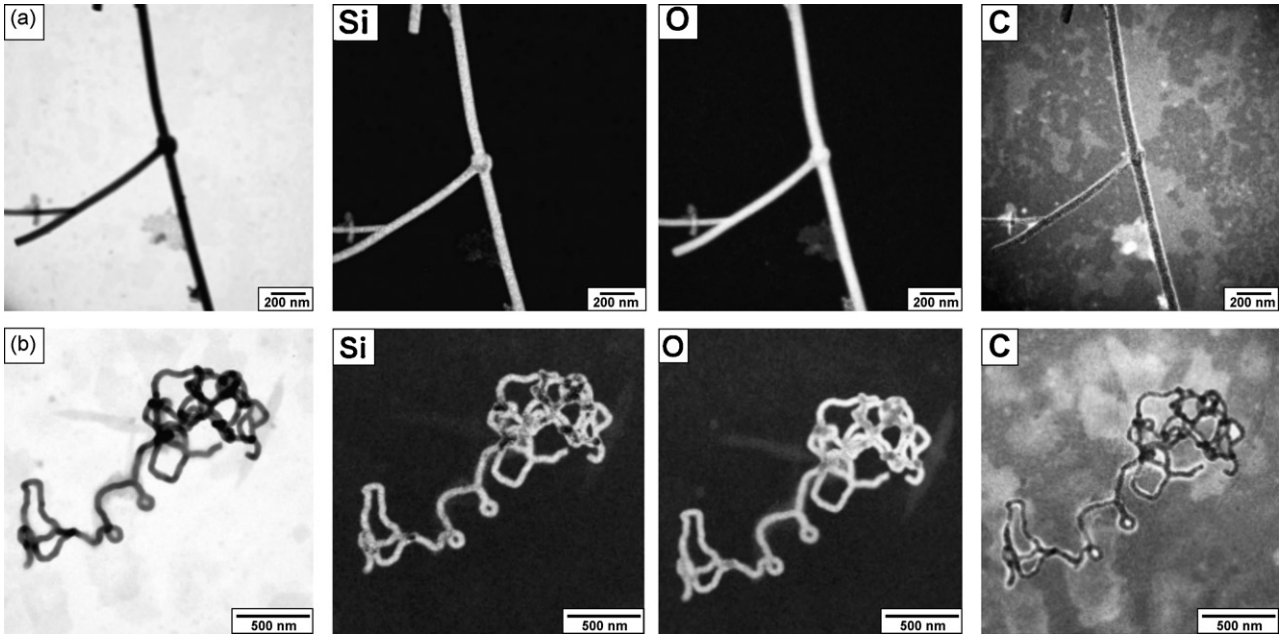

Fig. 7. Bright-field TEM images of the straight (a) and curved (b) nanowires together with the corresponding silicon, oxygen and carbon maps.

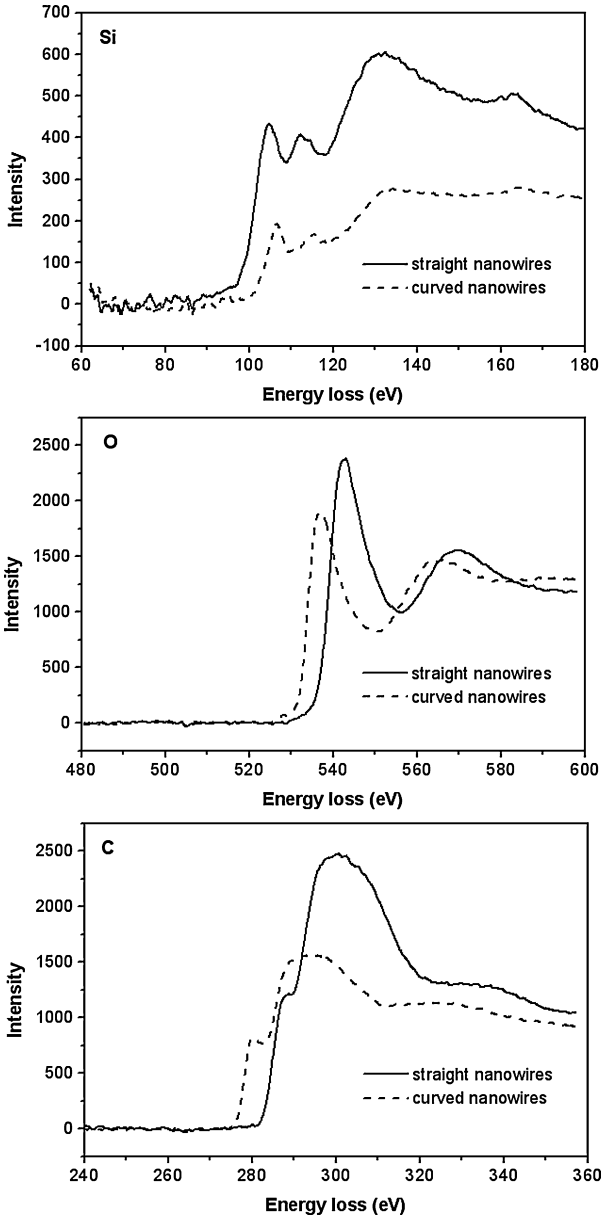

Fig. 8. EELS spectra for Si, O and C obtained from straight and curved nanowires.

nanowires and this value indicates that changes in the chemical environments of oxygen may have occurred. The spectrum gives a characteristic fine structure of the K-edge, which is due to the excitation of 1 s electrons into unoccupied p-like states. The oxygen K-edge for straight nanowires presented an onset at about 533 eV and showed two distinct peaks at 543 eV (α) and 570 eV (γ). The onset and the two peaks verified in the oxygen spectrum for SiO_2 were found to be at 524, 532 and 550 eV, respectively.[34] Both nanowires showed the presence of silicon, oxygen and carbon in their structures. As silicon is tetrahedrally coordinated, mixed SiC_xO_{4-x} units may be present, resulting in silicon sites such as SiC_4, SiC_3O, SiC_2O_2, $SiCO_3$ and SiO_4. Thus, the observed shift in the oxygen spectra may be related to these different sites. However, up to now it is not possible to identify which oxygen of which silicon site was more affected.

The carbon spectrum for straight nanowires also showed a shift of 7 eV in comparison with the curved nanowires, which may be associated to different critical ionization energies due to different chemical bonding states. The spectrum for straight nanowires showed an onset at 281 eV, a distinct π^* peak at 287 eV, associated with carbon in an sp^2 environment, and a broader σ^* peak at 300 eV, corresponding to the presence of sp^3-C sites in the structure.[33,35] It has been described that the carbon K-edge of SiC has an onset at 283 eV with two minor peaks at 286 and 296.5 eV and a major peak at 291 eV. In addition, two peaks with similar intensities are positioned at 305 eV and 315 eV.[32] For graphite, however, the carbon K-edge has an onset at 281 eV, a π^* peak centered at 285 eV and another peak at 292 eV. A broad peak at about 311 eV is also observed in graphite.[36] The area ratio, which provides an indirect evaluation of the sp^2/sp^3 bonding ratio,[33] for straight and curved nanowires was performed using Gaussian curve fitting. The straight nanowire presented a π^*/σ^* ratio of 2.34 while, for the curved nanowire, it was 3.26. Thus, straight nanowires presented a higher contribution of sp^3-C sites, while the curved nanowires revealed a relatively higher amount of sp^2-C sites in their structure.

As described earlier, the morphological analyses performed by SEM and TEM indicated that the nanowires produced in this study were not grown by the VLS mechanism, due to the absence of typical features of this mechanism. It is well known that SiC_xO_y ceramic decomposes at temperatures higher than ~1200 °C, with evolution of SiO and CO gases.[33] These gases can promote the following reactions:

$$SiO_{(v)} + 2CO_{(v)} \rightarrow SiC_{(s)} + CO_{2(v)} \quad (1)$$

$$2SiO_{(v)} + CO_{(v)} \rightarrow SiO_{2(s)} + SiCO_{(s)} \quad (2)$$

In this way, the nanowire growth mechanism may be correlated to the composition of the gaseous phase in SiO and CO gases, followed by a nucleation process, similar to the VS mechanism. The nanowire nature probably depends on the relative amount of these gases during the pyrolysis process, in which the product from reaction (1) results in a less flexible structure than that from reaction (2).

4. Conclusions

In the present study, the morphology of SiC_xO_y-based ceramics derived from a phenyl-rich hybrid polymer, prepared with and without Ni, has been described. The pyrolysis temperature was shown to be an important parameter to define the morphology and composition of the ceramic phases.

The increase of the pyrolysis temperature from 950 to 1500 °C led to densification and crystallization of SiC and graphite nanodomains in the ceramic bulk, as identified by HRTEM. In addition, the highly dispersed Ni-particles in the ceramic matrix obtained at 1500 °C produced relatively high amounts of nanowires with straight and curved morphologies, mainly on the ceramic specimen surface. Morphological characterization of the resulting nanowires, performed by EELS–TEM, indicated that Si and O elements are uniformly distributed in their structures and C is only present at the external lay-

ers. The nanowire growth is proposed to be similar to the VS mechanism and its respective nature was correlated to the relative compositions of the gases produced during the organic-to-inorganic transformation. It can be concluded that the presence of NiAc in the polymeric precursor was effective for inducing nanowire formation with different morphologies in the ceramic products when compared to ceramics prepared without Ni.

Acknowledgements

We gratefully acknowledge the financial support from FAPESP (Processes 05/58460-0 and 03/09926-1) and CNPq (Proc. 305916/2006-8). The authors also thank the Laboratório Nacional de Luz Síncrotron (LNLS) for HRTEM analyses and Prof. Dr. Carol H. Collins for English revision.

References

1. Riedel, R., Materials science and technology. In *A Comprehensive Treatment*, ed. R. W. Cahn, P. Haasen and E. J. Kramer. VCH, Weinheim, 1996, pp. 1–50.
2. Riedel, R., Paasing, G., Schönfelder, H. and Brook, R. J., Synthesis of dense silicon-based ceramics at low temperatures. *Nature*, 1992, **355**, 714–717.
3. Greil, P., Polymer derived engineering ceramics. *Adv. Eng. Mater.*, 2000, **2**, 339–348.
4. Schiavon, M. A., Radovanovic, E. and Yoshida, I. V. P., Microstructural characterization of monolithic ceramic matrix composites from polysiloxane and SiC powder. *Powder Technol.*, 2002, **123**, 232–241.
5. Wei, Q., Pippel, E., Woltersdorf, J., Scheffler, M. and Greil, P., Interfacial SiC formation in polysiloxane-derived Si–O–C ceramics. *Mater. Chem. Phys.*, 2002, **73**, 281–289.
6. Belot, V., Corriu, R. J. P., Leclercq, D., Mutin, P. H. and Vioux, A., Thermal redistribution reactions in crosslinked polysiloxanes. *J. Polym. Sci. A*, 1992, **30**, 613–623.
7. Hourlier, D. B., Latournerie, J. and Dempsey, P., Reaction pathways during the thermal conversion of polysiloxane precursors into oxycarbide ceramics. *J. Eur. Ceram. Soc.*, 2005, **25**, 979–985.
8. Kleebe, H.-J., Turquat, C. and Sorarù, G. D., Phase-separation in an SiCO glass studied by transmission electron microscopy and electron energy-loss spectroscopy. *J. Am. Ceram. Soc.*, 2001, **84**, 1073–1080.
9. Monthioux, M. and Delverdier, O., Thermal behavior of (organosilicon) polymer-derived ceramics. V: main facts and trends. *J. Eur. Ceram. Soc.*, 1996, **16**, 721–737.
10. Trassl, S., Motz, G., Rössler, E. and Ziegler, G., Characterization of the free-carbon phase in precursor-derived Si–C–N ceramics. I. Spectroscopic methods. *J. Am. Ceram. Soc.*, 2002, **85**, 239–244.
11. Gregori, G., Kleebe, H.-J., Brequel, H., Enzo, S. and Ziegler, G., Microstructure evolution of precursors-derived SiCN ceramics upon thermal treatment at temperatures ranging between 1000 and 1400 °C. *J. Non-Cryst. Solids*, 2005, **351**, 1393–1402.
12. Scheffler, M., Greil, P., Berger, A., Pippel, E. and Woltersdorf, J., Nickel-catalysed in situ formation of carbon nanotubes and turbostratic carbon in polymer-derived ceramics. *Mater. Chem. Phys.*, 2004, **84**, 131–139.
13. Leu, I. C., Hon, M. H. and Lu, Y. M., Chemical vapor deposition of silicon carbide whiskers activated by elemental nickel. *J. Electrochem. Soc.*, 1999, **146**, 184–188.
14. Nahm, K. S., Mo, Y. H., Shajahan, Md. and Lee, S. H., Catalytic growth of semiconductor micro- and nano-crystals using transition metal catalysts. *Kor. J. Chem. Eng.*, 2002, **19**, 510–518.
15. Jou, S. and Hsu, C. K., Preparation of carbon nanotubes from vacuum pyrolysis of polycarbosilane. *Mater. Sci. Eng. B*, 2004, **106**, 275–281.
16. Yang, W., Miao, H., Xie, Z., Zhang, L. and An, L., Synthesis of silicon carbide nanorods by catalyst-assisted pyrolysis of polymeric precursor. *Chem. Phys. Lett.*, 2004, **383**, 441–444.
17. Yang, W., Xie, Z., Miao, H., Zhang, L. and An, L., Simultaneous growth of Si_3N_4 nanobelts and nanodendrites by catalyst-assisted crystallization of amorphous SiCN. *J. Cryst. Growth*, 2005, **276**, 1–6.
18. Haberecht, J., Krumeich, F., Stalder, M. and Nesper, R., Carbon nanostructures on high-temperature ceramics—a novel composite material and its functionalization. *Catal. Today*, 2005, **102–103**, 40–44.
19. Deng, S. Z., Li, Z. B., Wang, W. L., Xu, N. S., Zhou, J., Zheng, X. G. *et al.*, Field emission study of SiC nanowires/nanorods directly grown on SiC ceramic substrate. *Appl. Phys. Lett.*, 2006, **89** [023118-1–023118-3].
20. Liang, C. H., Meng, G. W., Chen, W., Wang, Y. W. and Zhang, L. D., Growth and characterization of TiC nanorods activated by nickel nanoparticles. *J. Cryst. Growth*, 2000, **220**, 296–300.
21. Lu, H.-Y., Chu, S.-Y. and Chang, C.-C., Synthesis and optical properties of well-aligned ZnS nanowires on Si substrate. *J. Cryst. Growth*, 2005, **280**, 173–178.
22. Ci, L. J., Zhao, Z. G. and Bai, J. B., Direct growth of carbon nanotubes on the surface of ceramic fibers. *Carbon*, 2005, **43**, 883–886.
23. Djurisic, A. B., Tam, K. H., Hsu, Y. F., Zhang, S. L., Xie, M. H. and Chan, W. K., GaN nanowires–influence of the starting material on nanowire growth. *Thin Solid Films*, 2007, **516**, 238–242.
24. Berger, A., Pippel, E., Woltersdorf, J., Scheffler, M., Cromme, P. and Greil, P., Nanoprocesses in polymer-derived Si–O–C ceramics: electronmicroscopic observations and reaction kinetics. *Phys. Status Solidi (a)*, 2005, **202**, 2277–2286.
25. Segatelli, M. G., Pires, A. T. N. and Yoshida, I. V. P., Synthesis and structural characterization of carbon-rich SiC_xO_y derived from a Ni-containing hybrid polymer. *J. Eur. Ceram. Soc.*, 2008, **28**, 2247–2257.
26. Reimer, L., Zepke, U., Moesch, J., Schulze-Hillert, St., Ross-Messemer, M., Probst, W. and Weimer, E., ed., *EELS Spectroscopy: A Reference Handbook of Standard Data for Identification and Interpretation of Electron Energy Loss Spectra and for Generation of Electron Spectrocopic Images*. Oberkochen, Carl Zeiss, 1992.
27. Li, K.-Z., Wei, J., Li, H.-J., Li, Z.-J., Hou, D.-S. and Zhang, Y.-L., Photoluminescence of hexagonal-shaped SiC nanowires prepared by sol–gel process. *Mater. Sci. Eng. A*, 2007, **460–461**, 233–237.
28. Kleebel, H. –J. and Blum, Y. D., SiOC ceramic with high excess free carbon. *J. Eur. Ceram. Soc.*, 2008, **28**, 1037–1042.
29. Li, H. J., Li, Z. J., Meng, A. L., Li, K. Z., Zhang, X. N. and Xu, Y. P., SiC nanowire networks. *J. Alloys Compd.*, 2003, **352**, 279–282.
30. Yao, X., Tan, S., Huang, Z., Dong, S. and Jiang, D., Growth mechanism of β-SiC nanowires in SiC reticulated porous ceramics. *Ceram. Int.*, 2007, **33**, 901–904.
31. Egerton, R. F., *Electron Energy-Loss Spectroscopy in the Electron Microscopy*. Plenum, New York, 1986 [chapter 2].
32. Kaneko, K. and Kakimoto, K.-I., HRTEM and ELNES analysis of polycarbosilane-derived Si–C–O bulk ceramics. *J. Non-Cryst. Solids*, 2000, **270**, 181–190.
33. Gregori, G., Kleebe, H.-J., Blum, Y. D. and Babonneau, F., Evolution of C-rich SiOC ceramics. Part II. Characterization by high lateral resolution techniques: electron energy-loss spectroscopy, high-resolution TEM and energy-filtered TEM. *Int. J. Mater. Res.*, 2006, **97**, 710–720.
34. Lichtenberger, O. and Neumann, D., A study of Si–L and O–K ELNES in plant material: SiO_2, Ca– and Zn–silicate in Minuartia. *J. Microsc.*, 1996, **183**, 45–52.
35. Zhang, H. Z., Wang, R. M., You, L. P., Yu, J., Chen, H., Yu, D. P. *et al.*, Boron carbide nanowires with uniform CN_x coatings. *New J. Phys.*, 2007, **9**, 13–21.
36. Pamplin, B. R., *Crystal Growth* (*2nd ed.*). Pergamon Press, Oxford, 1980, p. 58.